



Impact of particles tracking model of nanofluid on forced convection heat transfer within a wavy horizontal channel

A.I. Alsabery^{a,b,*}, A. Hajjar^c, M.A. Sheremet^d, M. Ghalambaz^{e,f}, I. Hashim^b

^a Refrigeration & Air-conditioning Technical Engineering Department, College of Technical Engineering, The Islamic University, Najaf, Iraq

^b Department of Mathematical Sciences, Faculty of Science & Technology, Universiti Kebangsaan Malaysia, 43600 UKM, Bangi, Selangor, Malaysia

^c ECAM Lyon, LabECAM, Université de Lyon, Lyon, France

^d Department of Theoretical Mechanics, Tomsk State University, 634050 Tomsk, Russia

^e Department for Management of Science and Technology Development, Ton Duc Thang University, Ho Chi Minh City, Viet Nam

^f Faculty of Applied Sciences, Ton Duc Thang University, Ho Chi Minh City, Viet Nam

ARTICLE INFO

Keywords:

Forced convection
Nanofluids
Wavy horizontal channel
Nanoparticle tracking
Channel waviness

ABSTRACT

Development of modern heat exchangers or solar collectors is related to the analysis of working fluid flow and heat transfer within different channels. The energy transport enhancement can be reached by including nanofluids as working media and irregular channels to intensify the heat removal. The present research is devoted to computational analysis of nanosuspension forced convection in a horizontal wavy channel under the impact of heating from the upper wavy surface. The single-phase nanofluid approach with experimentally-based correlations for viscosity and thermal conductivity holds implemented for an investigation in combination with Newton's second law for the description of the motion of the nanoparticle within the channel. The formulated boundary-value problem has been worked out by the finite element technique. Rules of Reynolds number, number of channel waviness, and dimensionless time on nanofluid flow, energy transport and nanoparticles motion within the channel as well as average parameters. It has occurred that a rise from Reynolds number characterizes a narrowing of the fluid tube within the channel with an improvement of the average velocity and average Nusselt number. Augmentation of the channel waviness number results in an increment of the average particles velocity and average temperature.

1. Introduction

Nowadays, one of the major challenges in engineering fields is energy transport enhancement. A solution to this problem can be performed by the improvement of the working fluid or modification of the technological domains. In the first case, many researchers study an opportunity to use nanofluids as a combination of conventional thermal fluid with nano-sized particles of metal or metal oxide [1–3]. While in the second case, the modification of the considered region using fins, obstacles, irregular borders can be used [4–10]. Combination of these techniques can be very effective [11].

There are many published papers on nanofluid or non-Newtonian fluid flow in irregular channels [12,13]. Thus, Bahiraei et al. [12] have studied numerically a copper-water nanofluid flow, heat transfer and entropy production in a 3D ribbed channel using two-phase

mixture approach. Calculations have been performed using commercial CFD code Fluent. Authors showed that usage of nanofluid allows diminishing the irreversibility. At the same time, the entropy production can be reduced with a rise of the rib height. Mosayebidorcheh and Hatami [14,15] have scrutinized peristaltic nanofluid motion in a 2D wavy channel analytically. During an investigation, authors have found that low nanoparticles concentration characterizes a formation of maximum velocity and minimum temperature within channel. Using the commercial CFD code Fluent, Dormohammadi et al. [16] have examined energy transport and entropy production of copper-water nanofluid in 2D wavy channel. A single-phase nanofluid approach with Brinkman and Maxwell correlations allows modeling the waviness amplitude, Richardson number and nanoparticles concentration on flow structure, energy transport and entropy production. Authors have revealed the energy transport and entropy production enhancement with

* Corresponding author at: Refrigeration & Air-conditioning Technical Engineering Department, College of Technical Engineering, The Islamic University, Najaf, Iraq.

E-mail address: alsabery_a@ukm.edu.my (A.I. Alsabery).

<https://doi.org/10.1016/j.icheatmasstransfer.2021.105176>

nanoparticles concentration, while a rise of the Richardson number characterizes a reduction of the total entropy generation. Using the finite volume method with Semi-Implicit Method for Pressure Linked Equations-Consistent (SIMPLEC) algorithm, Alrashed et al. [17] have computed laminar nanofluid flow and energy transmission in 2D horizontal backward-facing contracting channel. The single-phase nanofluid model was employed for analysis. Authors have shown that an inclusion of nanoparticles increases the average Nusselt number, while fluid friction and pressure drop are raised more active for high Reynolds number. Some interesting results on nanofluid flow in corrugated channels can be found also in [18–22].

An insertion of porous medium within channels can allow intensifying the heat transport [23,24]. Thus, Alhajaj et al. [23] numerically and experimentally have examined nanofluid flow in porous channels for various flow rates and heat fluxes. Calculations have been performed using commercial CFD code Comsol Multiphysics. During an analysis authors have shown that the hybrid nanofluid utilization allows enhancing the energy transport performance in comparison with mono nanofluid. At the same time the friction factor and pressure drop are high for the hybrid nanofluid. An investigation of MHD copper-water nanofluid flow and energy transference in a partially porous wavy channel under the constant heat flux influence has been conducted using lattice Boltzmann technique by Ashorynejad and Zarghami [24]. It has been shown that an addition of nanoparticles enhances the heat transmission, while high porous medium permeability and thermal conductivity characterize a growth of the heat transfer strength.

In the case of intensive nanofluid motion the turbulent flows should be studied [25,26]. Thus, Manca et al. [25] have numerically scrutinized the turbulent flow and heat transfer of alumina-water nanofluid in 2D ribbed channel. The single-phase nanofluid model with SST $k - \omega$ turbulence approximation has been worked out using the finite volume technique with SIMPLE procedure. Authors have revealed that an inclusion of nanoparticles enhances the thermal transmission factor and pressure drop. An addition of turbulators leads to the heat transfer enhancement and pressure drop augmentation. Andreozzi et al. [26] have expanded the previous research [25] for the case of different rib shapes. As a result, the authors have shown that trapezoidal ribs have small heat transfer strength in comparison with the triangular ribs, but trapezoidal ribs characterize essentially low losses. Rajabi et al. [27] have investigated the turbulent nanofluid motion in a narrow channel with a spherical dimple employing the single-phase and two-phase approaches. SST $k - \omega$ turbulence approximation has been applied for analysis of hydrodynamics where in the combination with motion and energy equations the finite volume technique has been implemented. Authors have shown a presence of differences in results obtained using single-phase and two-phase techniques.

An inclusion of nanoparticles enhances the friction factor and heat transfer coefficient. Experimental examination of turbulent motion of hybrid nanosuspension consisting of water, graphite (40%) and silicon dioxide (60%) in a smooth tube with and without twisted tape has been conducted by Dalkilic et al. [28]. It has been revealed that a rise of nanoparticles volume fraction and twisted tape length enhance the heat transmission factor and the pressure drop. Khoshvaght-Aliabadi and Salami [29] have conducted a computational research of turbulent alumina-water nanofluid flow in offset-strip channel under the influence of constant heat flux from the channel walls. RNG $k - \epsilon$ turbulence approximation has been employed for investigation of liquid circulation where in the combination with motion and energy equations the finite volume technique has been accomplished. The authors have ascertained that the thermal transmission factor and pressure drop are high for the strip channel on comparison with smooth one. Moreover, the thermal performance factor can be enhanced with an addition of nanoparticles.

Ajeel et al. [30,31] have calculated the thermal and flow parameters for turbulent nanofluid circulation in a 3D trapezoidal-corrugated channel under various nanoparticles material and four nano-sized particles concentrations in the presence of constant heat flux boundary

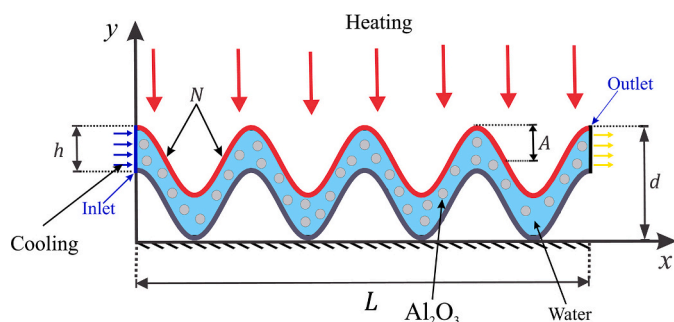


Fig. 1. 2D-Schematic description regarding the physical representation.

conditions. Commercial CFD code (Ansys-Fluent) has been used for solution to the motion and energy equations combined with standard $k - \epsilon$ turbulence model. The single-phase nanosuspension approach with Brownian effect has been applied. The obtained results have shown that the corrugated channel can enhance the thermal transmission factor in comparison with the straight channel. Moreover, the silicon dioxide-water nanofluid has been defined as an effective working medium for the considered regimes. Parsaiemehr et al. [13] have computed the turbulent flow and heat transmission of alumina/water nanofluid in 2D rectangular channel having inclined rectangular adiabatic ribs. Using the finite volume technique with SIMPLEC procedure authors solved the governing equations containing based on the single-phase nanofluid approach and SST $k - \omega$ turbulence approximation. The obtained results have demonstrated that the usage of the internal ribs is more essential in comparison with nanofluid, while a combination of such methods for the energy transport intensification allows increasing the heat transfer strength.

The presented brief review shows that nanofluid flow in corrugated channels is a crucial and practically-oriented topic. Moreover, in different engineering fields, including heat exchangers, chemical and nuclear reactors, the time can be considered as a major parameter reflecting the evolution of the energy transport process. The novelty of the present study is a detailed analysis of unsteady laminar nanofluid flow in a wavy channel using the second Newton's law for the description of the motion of the particles. Effect of the Reynolds number, waviness number, and dimensionless time on flow structures and heat transport is studied.

2. Mathematical formulation

Examine the unsteady convective heat transfer problem within a 2D wavy horizontal channel with length L and thickness (h), is reported in Fig. 1. The heat source is located at the upper wavy surface with fixed temperature (T_h), while the lower surface is assumed to be adiabatic. The inlet flow with cold temperature (T_c) inserts toward the wavy channel from the left vertical surface and uniform horizontal velocity (u_{in}). While the outlet fluid flow is moved from the right vertical surface with constant pressure ($p = 0$). The edges of the region remain impermeable, and the range within the wavy channel surfaces does filled by water- Al_2O_3 nanofluids. Concerning the hypotheses discussed above, the Navier-Stokes and energy equations of the Newtonian fluid do formulated as the following:

$$\nabla \cdot \mathbf{v} = 0, \quad (1)$$

$$\rho_{nf} \frac{\partial \mathbf{v}}{\partial t} + \rho_{nf} \mathbf{v} \cdot \nabla \mathbf{v} = -\nabla p + \nabla \cdot (\mu_{nf} \nabla \mathbf{v}), \quad (2)$$

$$(\rho C_p)_{nf} \left[\frac{\partial T}{\partial t} + \mathbf{v} \cdot \nabla T \right] = -\nabla \cdot (k_{nf} \nabla T), \quad (3)$$

where \mathbf{v} is the fluid velocity vector (U, V).

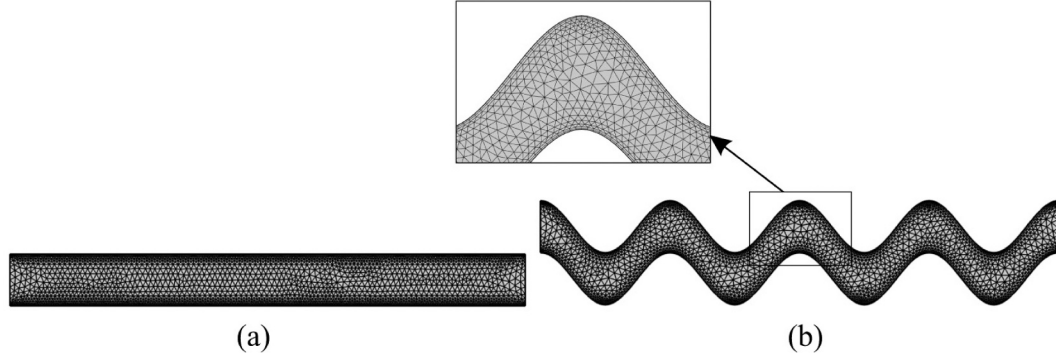


Fig. 2. Grid-points distribution for (a) horizontal straight channel with grid size of 5142 elements and (b) horizontal wavy channel with grid size of 4308 elements.

The particle positions are computed by solving second-order equations of motion for the particle position vector components, following Newton's second law,

Based on Newton's second law of motion, the governing equation of motion for the particles is given by:

$$\frac{d\mathbf{q}}{dt} = \mathbf{v}_p, \quad (4)$$

$$m_p \frac{d\mathbf{v}_p}{dt} = \mathbf{F}, \quad (5)$$

$$\mathbf{F} = \mathbf{F}_D + \mathbf{F}_T. \quad (6)$$

Where \mathbf{v}_p is the particle velocity. \mathbf{q} shows the particle position, m_p represents the particle mass and \mathbf{F} is the total force. \mathbf{F}_D and \mathbf{F}_T are the drag and thermophoretic forces and can be written as [32]:

$$\mathbf{F}_D = m_p \left(\frac{18\mu_f}{\rho_p d_p^2} \right) (\mathbf{v} - \mathbf{v}_p), \quad (7)$$

$$\mathbf{F}_T = - \frac{6\pi d_p \mu_f^2 C_s \Lambda \nabla T}{\rho_f (2\Lambda + 1) T}, \quad (8)$$

$$\Lambda = \frac{k_f}{k_p}, \quad C_s = 1.17. \quad (9)$$

The thermo-physical properties of Al_2O_3 -water nanofluid can be explained by the following:

$$(\rho C_p)_{nf} = (1 - \varphi)(\rho C_p)_f + \varphi(\rho C_p)_p, \quad (10)$$

$$\rho_{nf} = (1 - \varphi)\rho_f + \varphi\rho_p, \quad (11)$$

While the dynamic viscosity ratio of nanofluid for 33 nm particle-size is calculated as [33]:

$$\frac{\mu_{nf}}{\mu_f} = 1 / \left(1 - 34.87(d_p/d_f)^{-0.3} \varphi^{1.03} \right), \quad (12)$$

and the thermal conductivity ratio as [33]:

$$\frac{k_{nf}}{k_f} = 1 + 4.4Re_B^{0.4} Pr^{0.66} \left(\frac{T}{T_f} \right)^{10} \left(\frac{k_p}{k_f} \right)^{0.03} \varphi^{0.66}. \quad (13)$$

Where Re_B is evaluated as:

$$Re_B = \frac{\rho_f u_B d_p}{\mu_f}, \quad u_B = \frac{2k_b T}{\pi \mu_f d_p^2}. \quad (14)$$

Where φ is the local volume fraction of nanoparticles, T is the dimensional temperature, T_f shows the freezing point of the base fluid, $k_b = 1.380648 \times 10^{-23}(\text{J/K})$ is the Boltzmann constant. $l_f = 0.17\text{nm}$ is the mean path of fluid particles. d_f is the molecular diameter of water given as [33]:

$$d_f = 0.1 \left[\frac{6M}{N^* \pi \rho_f} \right]^{\frac{1}{3}}, \quad (15)$$

here M denotes the molecular weight of the base liquid, N^* means the Avogadro number and ρ_f signifies the density of the base liquid toward the regular temperature (310K).

Before the step of the solution, the governing equations do transform toward the dimensionless form, using the following dimensionless variables:

$$X = \frac{x}{L}, \quad Y = \frac{y}{L}, \quad \mathbf{V} = \frac{\mathbf{v}}{U_i}, \quad \theta = \frac{T - T_c}{T_h - T_c}, \quad (16)$$

$$Pr = \frac{\nu_f}{\alpha_f}, \quad Re = \frac{U_i L}{\nu_f}, \quad P = \frac{pL^2}{\rho_f \alpha_f^2},$$

where \mathbf{V} is the fluid velocity dimensionless vector, θ is the dimensionless temperature and P is the dimensionless pressure. The boundary conditions concerning the governing equations do addressed by:

At the hot upper wavy surface:

$$u = 0, v = 0, T = T_h, 0 \leq x \leq L, d - A(1 - \cos(N\pi y)), \quad (17)$$

At the cold inlet left surface:

$$u = u_m, v = 0, T = T_c, x = 0, 0 \leq y \leq h, \quad (18)$$

At the adiabatic lower wavy surface:

$$u = 0, v = 0, \frac{\partial T}{\partial Y} = 0, 0 \leq x \leq L, h - A(1 - \cos(N\pi y)), \quad (19)$$

At the adiabatic outlet right surface:

$$p = 0, \frac{\partial T}{\partial x} = 0, x = L, 0 \leq y \leq h, \quad (20)$$

where A and N show the amplitude and number of undulations. The local heat transfer (Nusselt number) does determine with the heated top wavy surface as the following:

$$Nu_{nf} = - \frac{k_{nf}}{k_f} \sqrt{\left(\frac{\partial \theta}{\partial X} \right)^2 + \left(\frac{\partial \theta}{\partial Y} \right)^2}. \quad (21)$$

and the average Nusselt number (\overline{Nu}_{nf}) can be calculated by integrating the local Nusselt number along the top wavy surface which is defined by

$$\overline{Nu}_{nf} = \frac{1}{W} \int_0^W Nu_{nf} dW. \quad (22)$$

where W shows the total length of the wavy top heater.

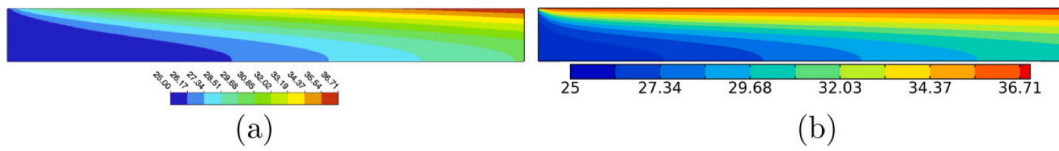


Fig. 3. Validations of isotherms contours for (a) Gorji and Ranjbar [35] and (b) present study for horizontal straight channel.

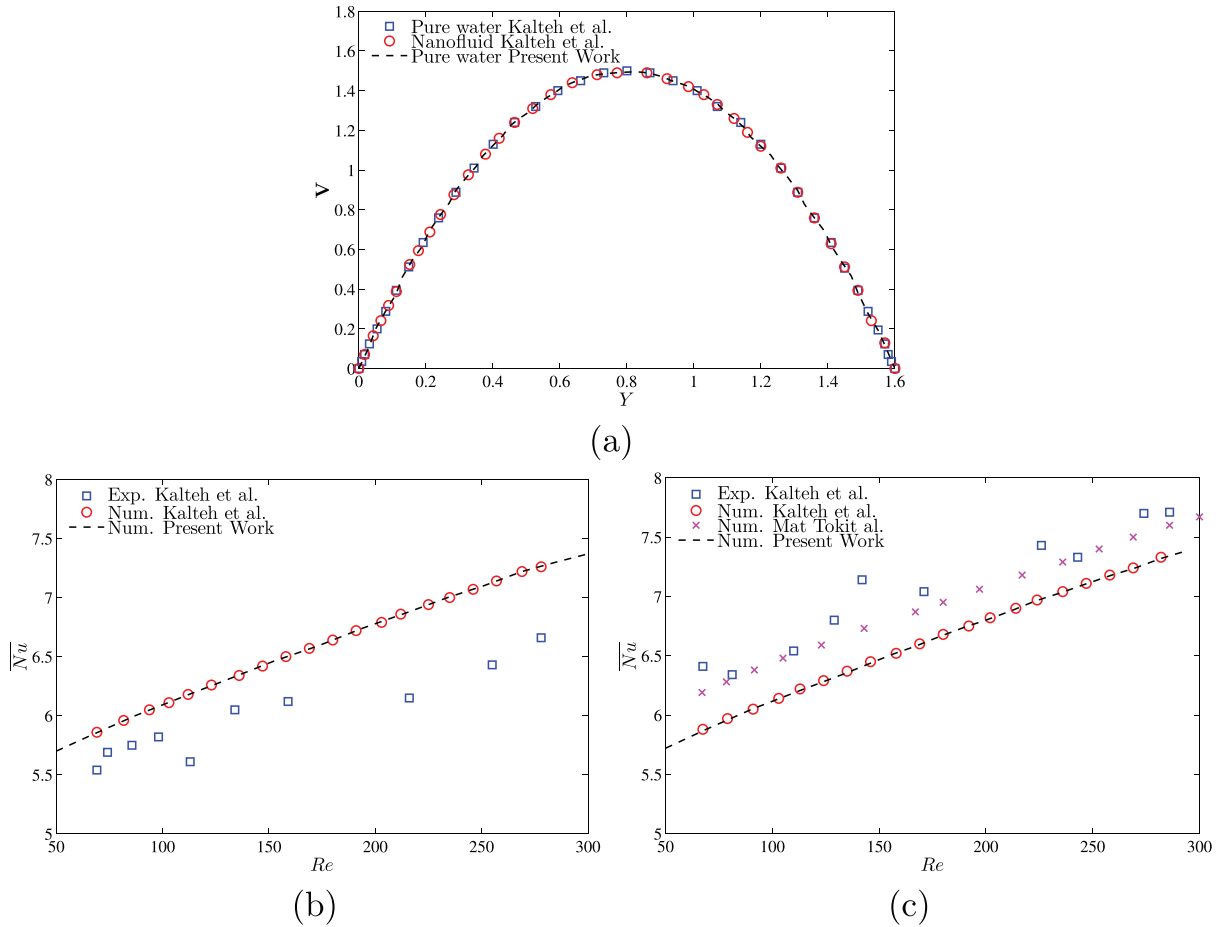


Fig. 4. Validations of (a) dimensionless velocity profile of the experimental and numerical results of Kalteh et al. [36] and the present result for pure fluid (water) and nanofluid of 0.01 Al_2O_3 nanoparticles at $Re = 300$, (b) average Nusselt numbers with Re of the experimental and numerical results of Kalteh et al. [36] and the present result for pure fluid and (c) average Nusselt numbers with Re of the experimental and numerical results of Kalteh et al. [36], Tokit et al. [37] and the present result for nanofluid of $(\phi = 0.01)$ using the single-phase model.

3. Numerical method and validation

The dimensionless governing equations and associated boundary conditions do solved among the Galerkin weighted residual finite-element procedure. The computational region was divided toward sub-domains (finite elements) (as given in Fig. 2) and the velocity distribution, pressure, temperature and the nanoparticle distribution exist approximated through adopting a basis valued of $\{\Phi_j\}_{j=1}^M$ as:

$$\begin{aligned}
 V &\approx \sum_{j=1}^M V_j \Phi_j(X, Y), & P &\approx \sum_{j=1}^M P_j \Phi_j(X, Y), & \theta &\approx \sum_{j=1}^M \theta_j \Phi_j(X, Y), \\
 \phi &\approx \sum_{j=1}^M \phi_j \Phi_j(X, Y),
 \end{aligned}
 \tag{23}$$

where Φ describes the base functions, and j expresses the internal nodes. Details of the finite element analysis are clearly outlined in Reddy [34]. Triangular Lagrange finite components regarding various orders stand to use toward any of the flow variables into the computational region.

Residuals toward any conservation equation are accomplished through replacing the approximations within the dimensionless governing equations. For clarifying the nonlinear expressions within the dimensionless momentum equations, the Newton-Raphson iteration algorithm is adopted. The convergence of the solution does appropriate during the relative error toward each of the variables meets the following convergence criteria:

Table 1
Thermo-physical properties of water and Al_2O_3 nanoparticles in $T = 310K$ [38].

Physical properties	Fluid phase (water)	Al_2O_3
$k(Wm^{-1}K^{-1})$	0.628	40
$\mu \times 10^6(kg/ms)$	695	-
$\rho(kg/m^3)$	993	3970
$C_p(J/kgK)$	4178	765
$\beta \times 10^5(1/K)$	36.2	0.85
$d_p(nm)$	0.385	33

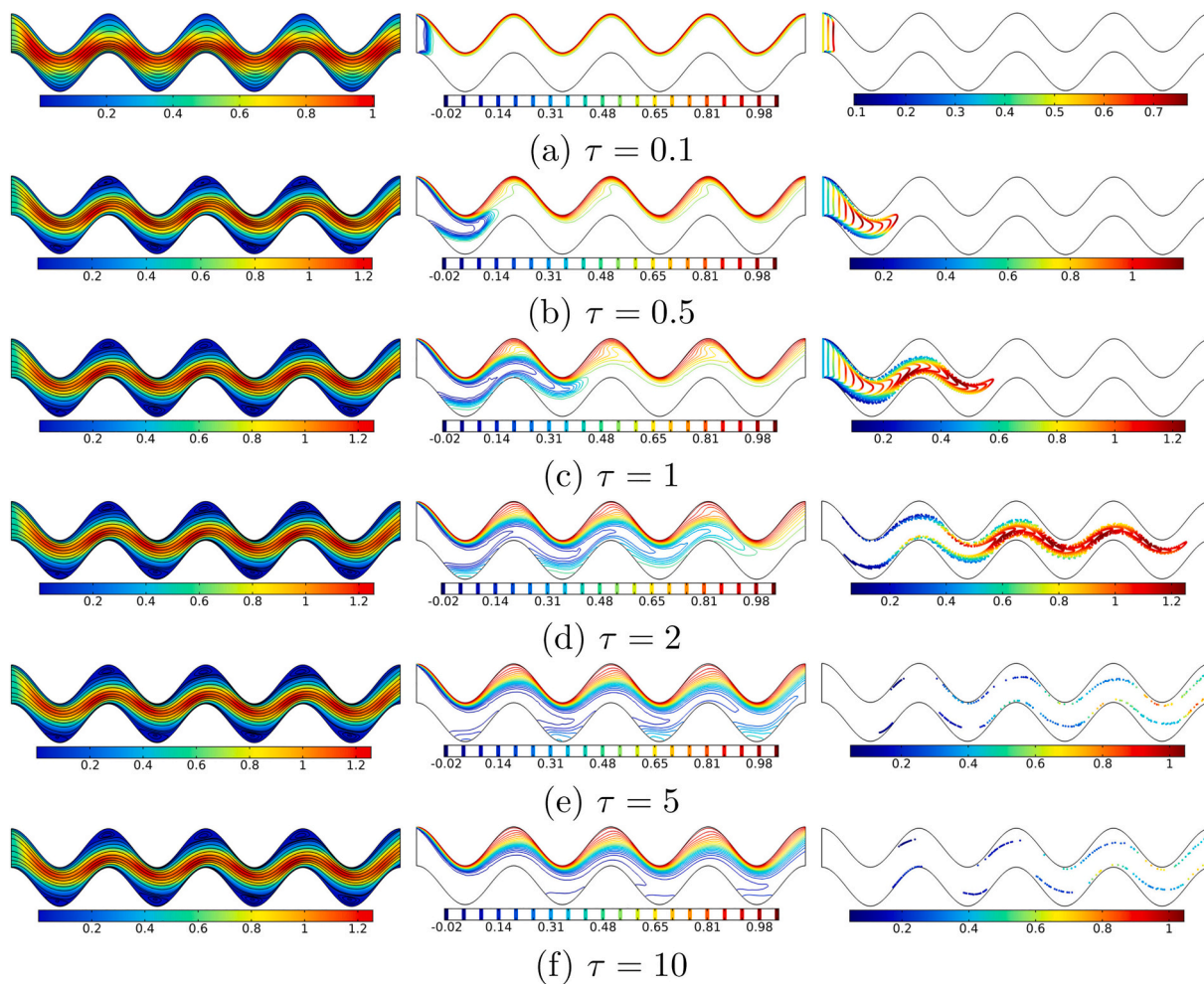


Fig. 5. Variations of (left) velocity (streamlines), (middle) isotherms, and (right) nanoparticle trajectories evolution by the dimensionless time (τ) for $Re = 500$ and $N = 4$.

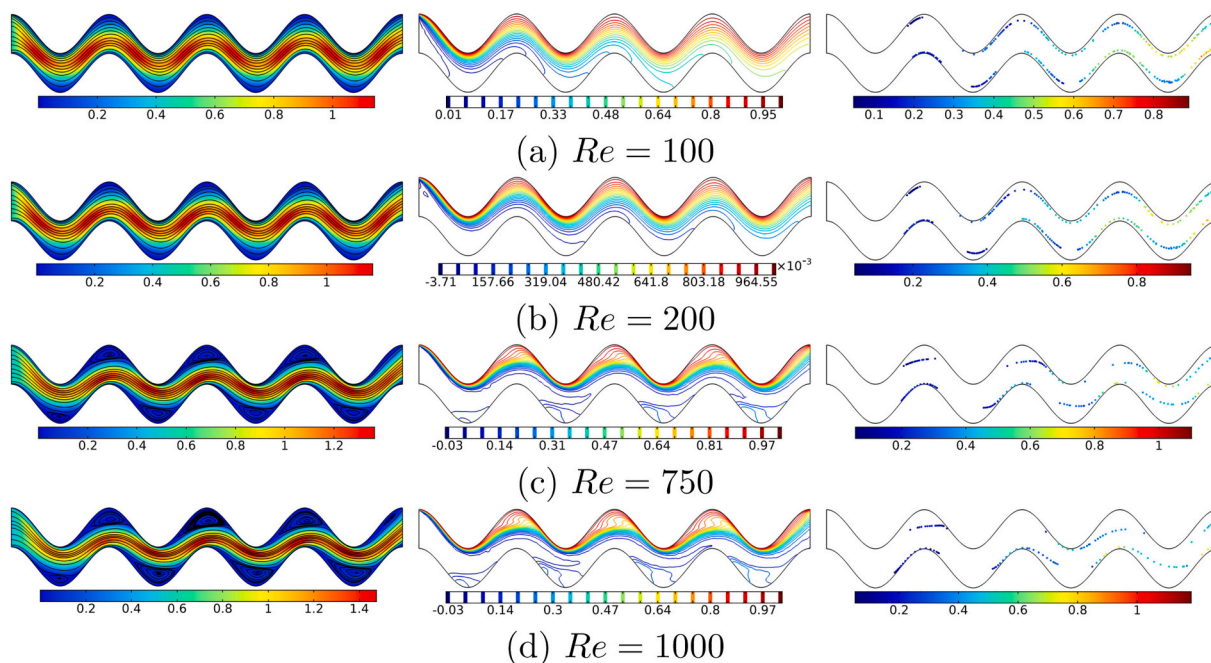


Fig. 6. Variations of (left) velocity (streamlines), (middle) isotherms, and (right) nanoparticle trajectories evolution by Reynolds number (Re) for $\tau = 10$ and $N = 4$.

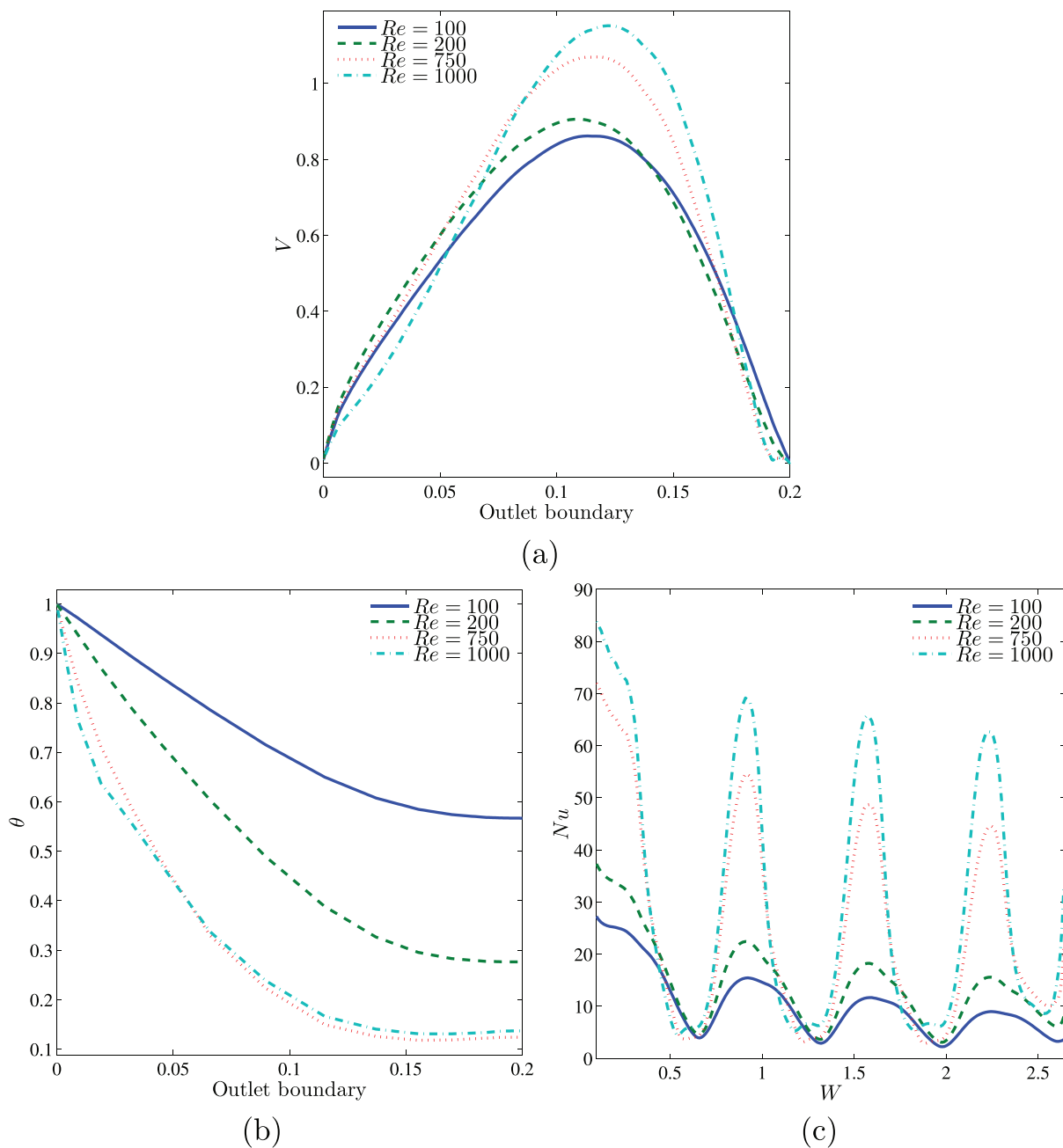


Fig. 7. Variations of (a) dimensionless velocity at the outlet boundary, (b) dimensionless local temperature at the outlet boundary and (c) local Nusselt number interfaces with the wavy heated wall W for different Re at $\tau = 10$ and $N = 4$.

$$\left| \frac{\Gamma^{i+1} - \Gamma^i}{\Gamma^{i+1}} \right| \leq \eta,$$

here i and η describe the iteration quantity and the convergence criterion, respectively.

Concerning the purpose of verifying the existing data, the outcomes from the current performance do associate among the findings described by Gorji and Ranjbar [35] toward the phenomena of forced convection within a horizontal straight channel heated from the top, as shown in Fig. 3. Also, comparisons are reported among the numerical data of the current work and the experimental and numerical works of Kalteh et al. [36] and Tokit et al. [37] toward the problem of forced convection heat transfer concerning alumina-water nanofluids into an extended rectangular microchannel heat sink, as revealed in Fig. 4. These outcomes contribute to confidence in the accuracy regarding the existing

numerical approach.

4. Results and discussion

This section presents numerical results for the streamlines, isotherms, and the isentropic lines for five parameters. These are dimensionless time ($0.001 \leq \tau \leq 10$), Reynolds number ($100 \leq Re \leq 1000$) and number of oscillations ($0 \leq N \leq 5$). The values of nanoparticle volume fraction, Prandtl number, the amplitude, thickness and total height of the channel are fixed at $\phi = 0.02$ (100 nanoparticles), $Pr = 4.623$, $A = 0.1$, $H = 0.2$ and $D = 0.4$, respectively. The thermo-physical properties of the base fluid (water) and the solid Al_2O_3 phases are tabulated in Table 1.

The time evolution of the streamlines, the isothermal contours, and the nanoparticle trajectories is shown in Fig. 5. At initial times, the

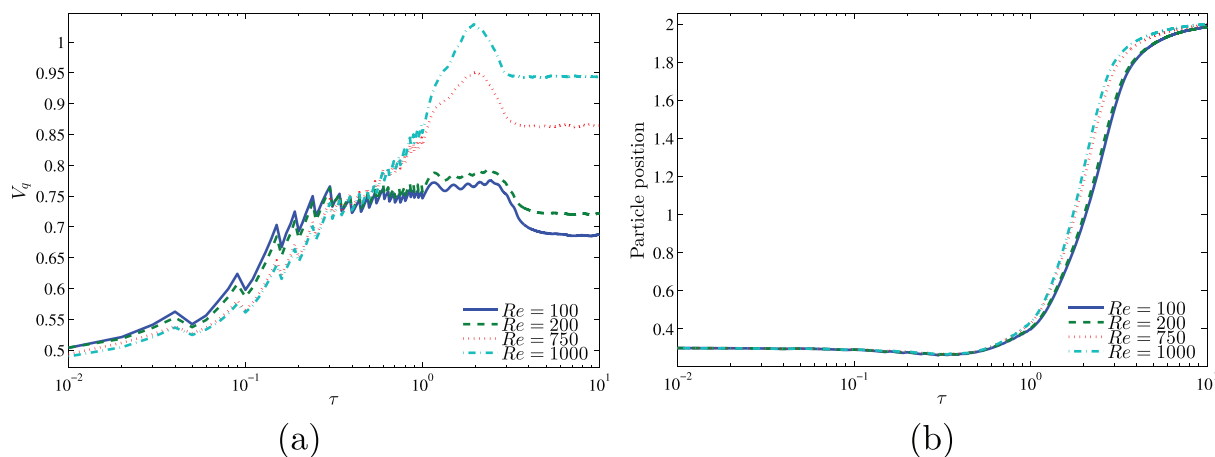


Fig. 8. Variations of (a) average particle velocity magnitude and (b) average particle position with τ for different Re at $N = 4$.

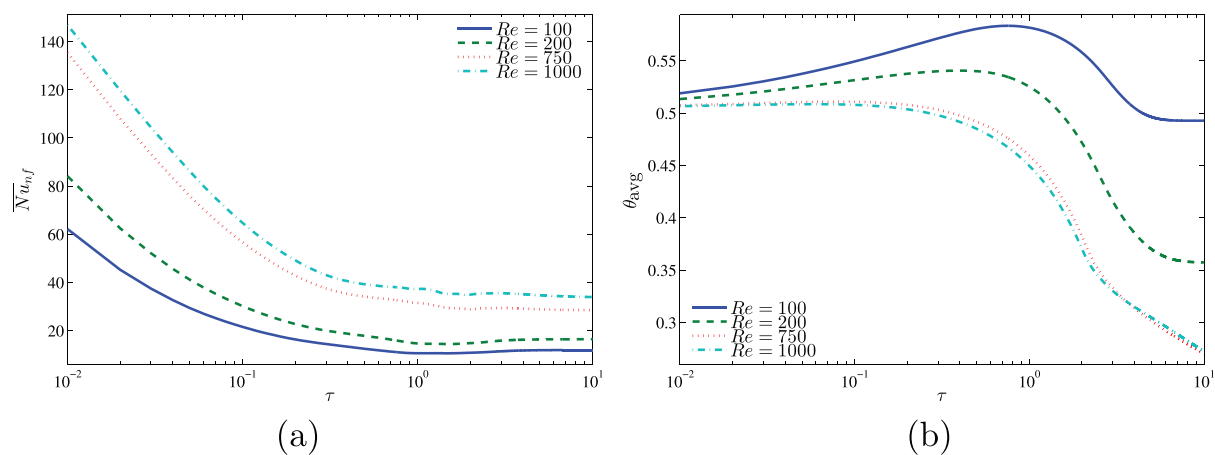


Fig. 9. Variations of (a) average Nusselt number and (b) with average dimensionless temperature with τ for different Re at $N = 4$.

streamlines are wavy and follow the wall periodic variation. As time goes, recirculation zones appear in the wavy wall crests, due to the disturbance of the flow by the geometrical wall variation and to the convective effects. At the same time, the maximum velocity remains concentrated in the middle of the channel. These recirculation zones are due to the fluid momentum mismatch between the fast-moving fluid in the channel center and the quasi-stagnant fluid in the furrows of the channel. The isotherms are affected by the flow patterns and the temperature difference between the heated wall and the liquid. The upper wall heats the cold fluid entering the channel, so the isothermal contours corresponding to high temperatures are wavy lines concentrated near the top wall and following the wall undulations. The fluid temperature reduces by moving from the top toward the channel center, and the cold temperature occupies the region between the channel center and the bottom wall.

The nanoparticles enter the channel for the left and start to move and occupying the whole height, and as time goes, they spread uniformly in the central region affected by the drag force. The thermophoretic force tends to push the particles vertically in a direction opposed to the temperature gradient, and, thus, the particles move away from the upper hot wall toward the center and from the center toward the bottom, without being trapped into the recirculation zones. So they finally focus into two migration zones, located just below and above the recirculation zones near the top and bottom walls respectively. The nanoparticles are therefore concentrated near the channel walls and their distribution is not uniform.

Fig. 6 illustrates the streamlines, the isotherms, and the trajectories

of the nanoparticles in the channel for different values of Reynolds number Re . For $Re = 100$, the flow is laminar, and the streamlines follow the channel undulation. As Re is increased, the flow near the wall crests is disturbed due to the higher inertial forces and increased flow velocity in the channel center, which leads to the appearance of recirculation zones near the wall crests. The intensity of the recirculation rises with Re and is maximum for $Re = 1000$. In addition, the recirculation is relatively less intense near the lower wall compared to the upper one, where convective heat transfer is playing an important role. The isotherms show that, for all the values of Re , the hot fluid is occupying the upper part of the channel, while the cold one is in the central and lower parts. The appearance of recirculation zones for higher Re disturbs the shape of the isotherms, mainly near the wavy wall crests. As for the nanoparticles, two migration lines can be seen for all the values of Re , just above and below the recirculation zones. Nonetheless, these lines are very close to the channel walls for low Re . However, the increase of the Reynolds number raises the size of the recirculation zones near the crests and pushes the particles away from the walls. Thus, the increase of Re shifts the migration lines closer to the channel center.

Fig. 7 shows the dimensionless velocity V and the dimensionless temperature θ at the outlet boundary, and the local Nusselt number (Nu) over the wavy wall for various values of Re . Here, V shows the same trend of variation for all the values of Re . It is zero at the channel walls due to the no-slip boundary condition and increases gradually to reach its maximum near the center. The value of this maximum elevates by the growth of Re , which boosts the entering flow velocity. It is also shown that the temperature θ over the outlet is reduced when Re is increased,

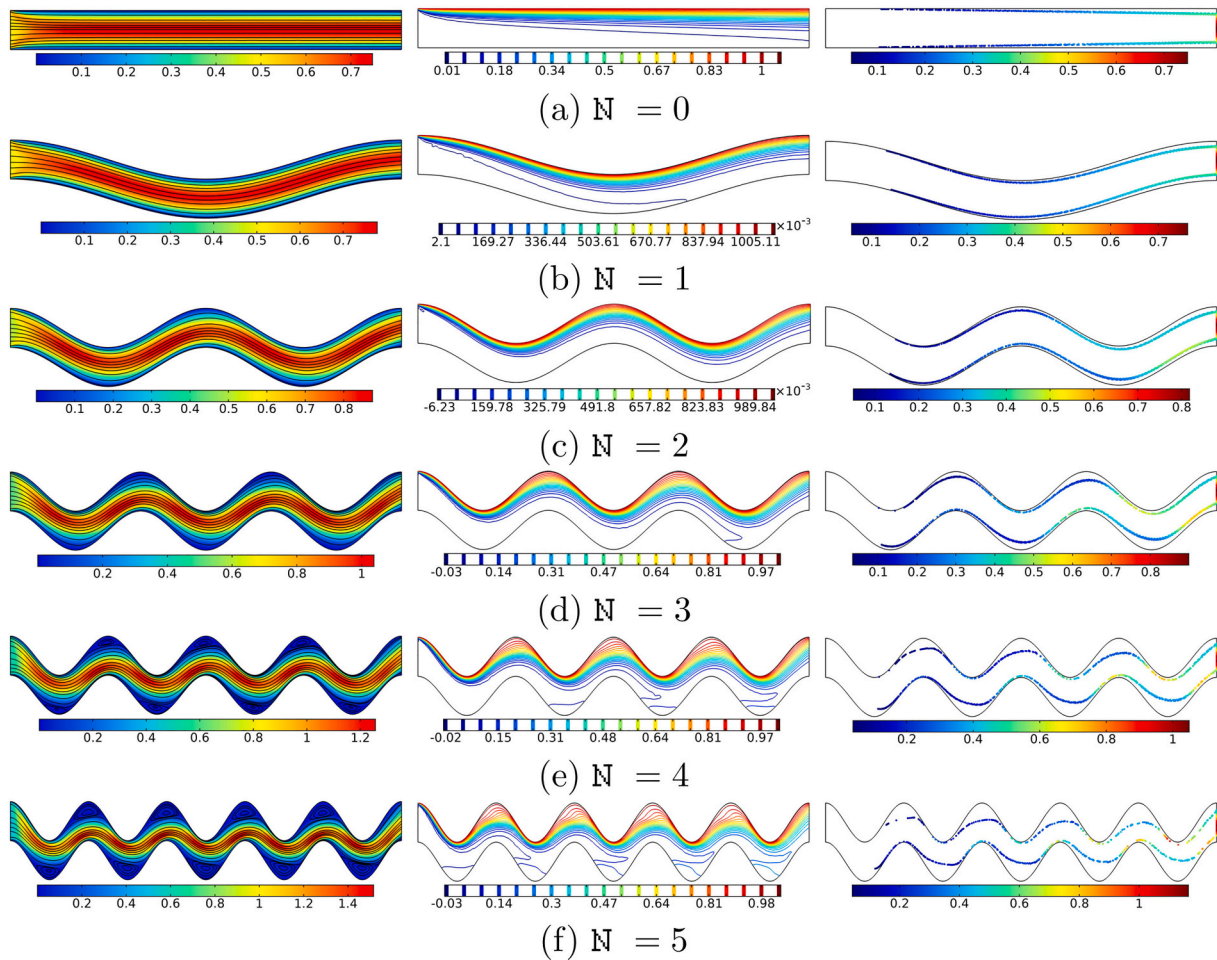


Fig. 10. Variations of (left) velocity (streamlines), (middle) isotherms, and (right) nanoparticle trajectories evolution by number of oscillations (N) for $\tau = 10$ and $Re = 500$.

indicating that the higher the value of Re , the colder the fluid will be when leaving the channel. In fact, this is mainly valid in the channel center and close to the lower wall and related to the flow isotherms, as displayed in Fig. 6. The Nusselt number (Nu) shows a periodic variation following the wavy wall, and its amplitude substantially increases when Re is raised, which shows an enhancement of the heat transfer rate over the heated wall for a higher Re . Indeed, the appearance of recirculation zones near the wall crests amplifies fluid mixing in that region and contributes to the heat transfer enhancement.

The variation of the average particle velocity (V_q) and the average particle position as functions of time for different values of Re is plotted in Fig. 8. It can be seen that V_q progressively increases with time. V_q is initially slightly higher for low Re ; then, as time goes, it starts to rise with Re and is maximum for $Re = 1000$. This is due to the reduction of the viscous effects compared to the inertial ones for higher Re combined with the increase of the flow entering velocity. The particle position is the same for all Re at the initial times, then a slight increase in the position appears when Re is raised. This is related to the results discussed in Fig. 6, as the increase of the size of the recirculation zones near the walls tends to lead the particles away from the walls toward the channel center. However, as this happens near the two walls, the final average position of the particles is almost the same for all the values of Re .

Fig. 9 depicts the variation of the average Nusselt number (\overline{Nu}_{nf}) and the average temperature (θ_{avg}) as functions of time for different values of Re . Here, \overline{Nu}_{nf} is always higher when Re is increased, indicating a more intense heat transfer, due to the intensification of inertial effects and the recirculation zones near the hot wavy wall. Simultaneously, θ_{avg} remains

lower when Re is increased due to the higher fluid velocity, and the reduction of θ_{avg} with Re becomes more significant as time goes.

The streamlines, isotherms, and particle trajectories are shown in Fig. 10 for different numbers of oscillations N . The case $N = 0$ corresponds to a channel with straight walls. In this case, the flow streamlines are straight lines symmetrical around the channel center, indicating low convective effects. Similar behavior can be seen for $N = 1$, corresponding to a curved channel. The effect of N starts to appear when it is increased above 2. The waviness of the walls disturbs the flow patterns, and recirculation zones start to appear next to the wall crests. The recirculation is intensified when N is increased. In fact, the distance between inlet and outlet is the same while the number of oscillation is increased, meaning that the wavelength of the walls is reduced. These walls are thus more corrugated and cause more disturbance to the flow field. The isotherms show similar behavior in all the cases, where the hot fluid occupies the upper region of the channel and concentrated near the crests of the upper wall. As for the nanoparticle trajectories, two migration lines are always present. The position of these lines shifts toward the channel center when a higher value of N is used, as the corrugation of the walls and the intensity of the recirculation are increased.

The effects of N on the dimensionless velocity V and the dimensionless temperature θ at the outlet boundary and on the local Nusselt number Nu over the wavy wall are illustrated in Fig. 11. Both the temperature θ and the maximum value of V raise when N is increased, and are minimum in a case of a channel with straight walls. Indeed, as the wall corrugation increases for higher N , the disturbance of the flow by

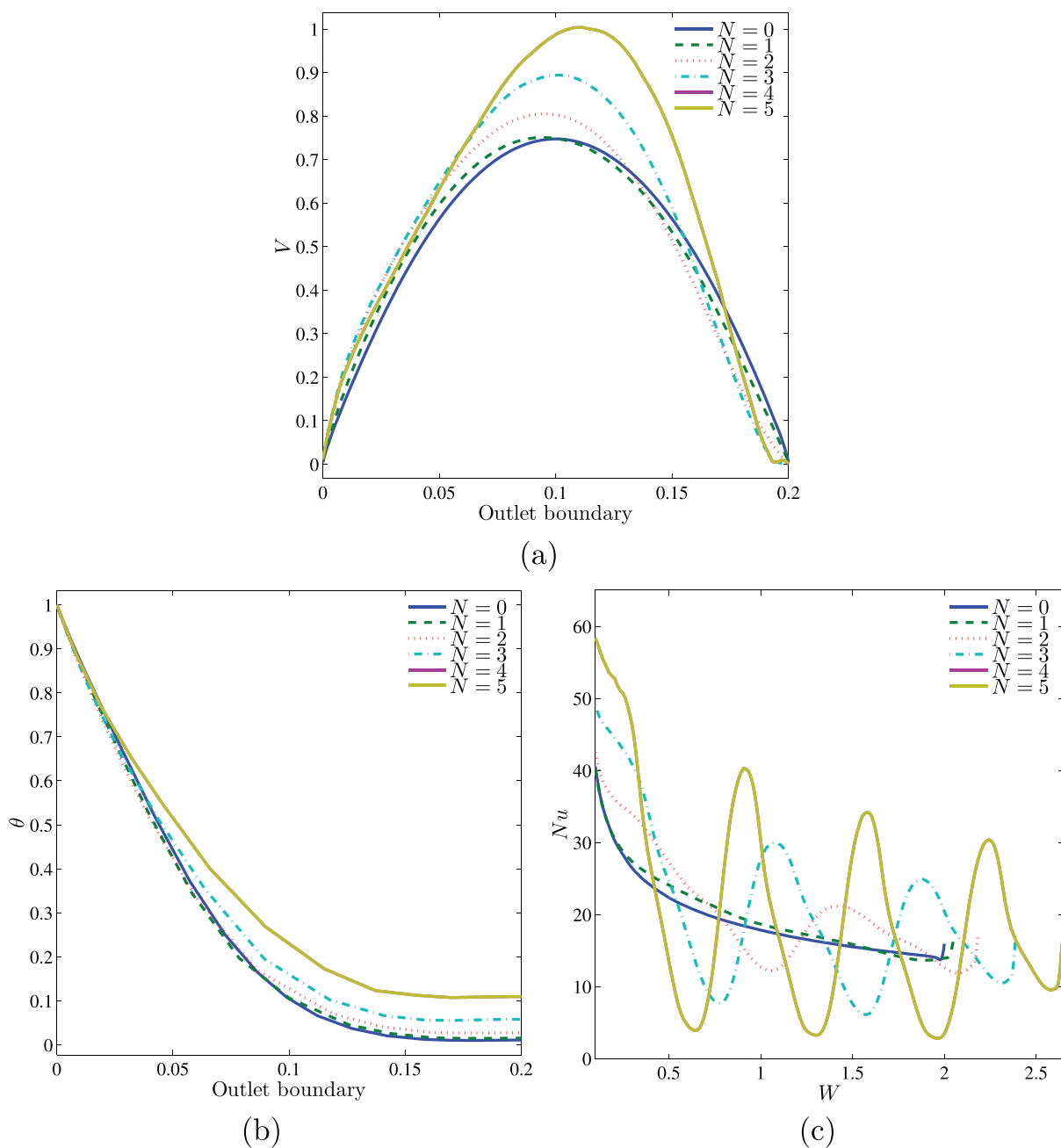


Fig. 11. Variations of (a) dimensionless velocity at the outlet boundary, (b) dimensionless local temperature at the outlet boundary and (c) local Nusselt number interfaces with the wavy heated wall W for different N at $\tau = 10$ and $Re = 500$.

the wavy walls increases the mismatch of the flow momentum between the channel center and the walls and leads to a higher velocity in the center of the channel. Moreover, the increase of the thermal boundary layer near the lower wall leads to a higher value of θ in that region. As for Nu , its variation follows that of the wall, so it is also alternating when the walls are wavy. The maximum of Nu significantly increases for higher values of N , due to the higher mixing in the recirculation zones near the wall crests. Nonetheless, the flow is faster near the wall troughs, and Nu shows a minimum in that region. This minimum decreases for a higher N . Overall, raising N seems to increase the mean value of Nu slightly.

Fig. 12 shows the variation of the average particle velocity V_q and the average particle position as functions of time for various values of N . Raising N increases the value of V_q and, to a less extent, the particle position. This is due, as discussed earlier, to the increase of the flow

velocity due to the growth of the wall corrugations for higher N . Also, the resulting intensification of the recirculation zones moves the particle position away from the channel walls. As this happens near the upper and bottom wall, the final average position of the particles remains almost unchanged for all the cases.

The variation of \overline{Nu}_{nf} and θ_{avg} as functions of time for different values of N is depicted in Fig. 13. Initially, \overline{Nu}_{nf} is higher for low N and is maximum in the case of straight walls. Nonetheless, as time goes, this trend changes due to the enhancement of fluid mixing near the wavy wall crests, and finally, \overline{Nu}_{nf} slightly increases when N is raised. θ_{avg} also rises with N over time, due to the growth of the thermal boundary layer near the bottom wall and is minimum in the case of straight walls.

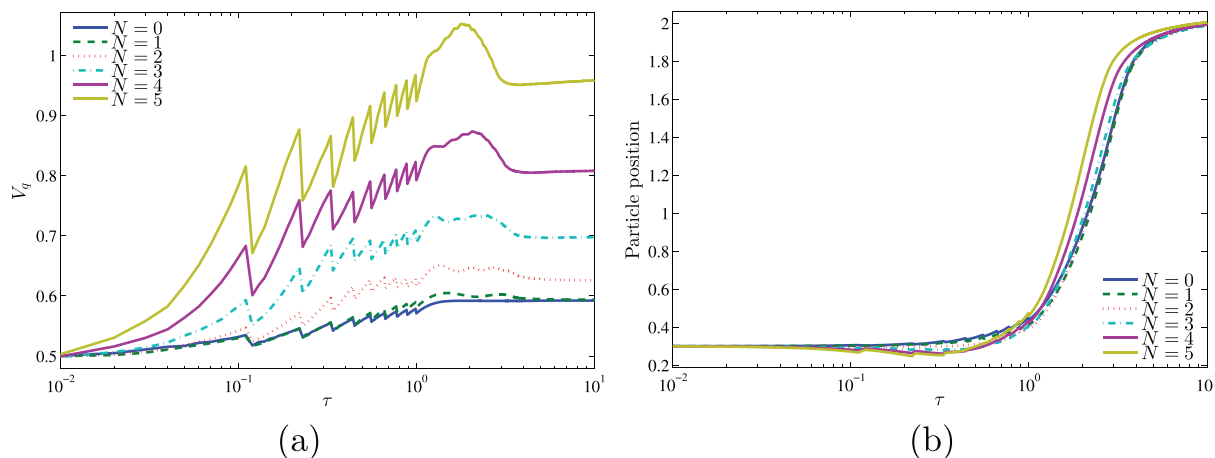


Fig. 12. Variations of (a) average particle velocity magnitude and (b) average particle position with τ for different N at $Re = 500$.

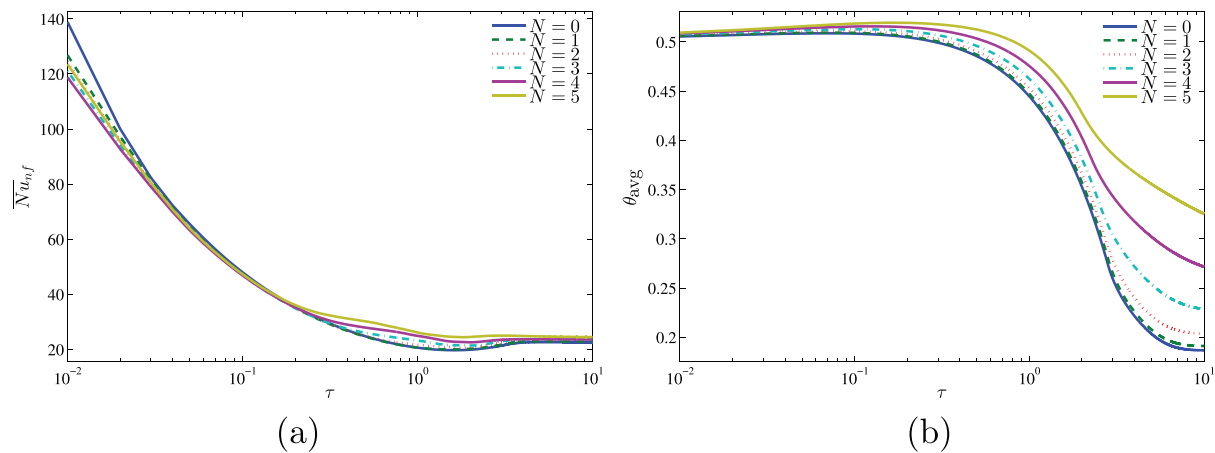


Fig. 13. Variations of (a) average Nusselt number and (b) average dimensionless temperature with τ for different N at $Re = 500$.

5. Conclusions

Toward the existing research, the flow and heat transfer of alumina-water nanofluids within a wavy-wall channel were examined numerically. The migration behavior of nanoparticles due to the drag and thermophoretic forces were addressed. The governing equations for conservation of mass, momentum, and energy were formed in the Eulerian system and solved numerically using FEM. Then, the flow and temperature fields were used to integrate the trajectory path of the nanoparticles in the Lagrange system. The effect of Reynolds number and wall wavy number (N) toward the flow and heat transfer and the particle paths were investigated. The primary findings concerning the existing computational investigation can be compiled as:

1. The nanoparticles migrate in the channel into two focusing lines near the upper and bottom surface, due to the impact of the thermophoretic force. The increase of recirculation zones near the walls crests tend to move the particles away from the walls toward the channel centre. So overall, the distribution of the nanoparticles is not uniform and mainly concentrated near the channel walls.
2. Increasing Re intensifies the mixing of the fluid near the channel surfaces and enhances heat transfer. For a higher Re , the average particle velocity increases, the particle trajectories move closer toward the channel centre, and the fluid leaves the wavy channel among below-average temperature.

3. A channel with a higher number of wavy wall oscillations presents a slight heat transfer rate due to increased wall corrugation and the resulting growth of fluid mixing. When N is raised, the average particle velocity increases, and the fluid leaves the channel with a higher average temperature.

Declaration of Competing Interest

On behalf of the co-authors, I declare that we don't have any conflict of interest.

Acknowledgments

We are grateful for the financial support received from the Malaysian Ministry of Education under the research grant FRGS/1/2019/STG06/UKM/01/2.

References

- [1] M.U. Sajid, H.M. Ali, Recent advances in application of nanofluids in heat transfer devices: a critical review, *Renew. Sust. Energ. Rev.* 103 (2019) 556–592.
- [2] M.H. Ahmadi, M. Ghazvini, M. Sadeghzadeh, M.A. Nazari, M. Ghalandari, Utilization of hybrid nanofluids in solar energy applications: a review, *Nano-Struct. Nano Objects* 20 (2019), 100386.
- [3] M.H. Esfe, M.H. Kamyab, M. Valadkhani, Application of nanofluids and fluids in photovoltaic thermal system: an updated review, *Sol. Energy* 199 (2020) 796–818.

- [4] W.R. Liao, L.H. Chien, M. Ghalambaz, W.M. Yan, Experimental study of boiling heat transfer in a microchannel with nucleated-shape columnar micro-pin-fins, *Int. Communicat. Heat Mass Trans.* 108 (2019), 104277.
- [5] N.S. Bondareva, M.A. Sheremet, Conjugate heat transfer in the pcm-based heat storage system with finned copper profile: application in electronics cooling, *Int. J. Heat Mass Transf.* 124 (2018) 1275–1284.
- [6] A.K. Asl, S. Hossainpour, M.M. Rashidi, M.A. Sheremet, Z. Yang, Comprehensive investigation of solid and porous fins influence on natural convection in an inclined rectangular enclosure, *Int. J. Heat Mass Transf.* 133 (2019) 729–744.
- [7] S.A.M. Mehryan, A. Alsabery, A. Modir, E. Izadpanahi, M. Ghalambaz, Fluid-structure interaction of a hot flexible thin plate inside an enclosure, *Int. J. Therm. Sci.* 153 (2020), 106340.
- [8] X. Zheng, Z. Qi, A comprehensive review of offset strip fin and its applications, *Appl. Therm. Eng.* 139 (2018) 61–75.
- [9] A.M. Abdulateef, S. Mat, J. Abdulateef, K. Sopian, A.A. Al-Abidi, Geometric and design parameters of fins employed for enhancing thermal energy storage systems: a review, *Renew. Sust. Energ. Rev.* 82 (2018) 1620–1635.
- [10] I.V. Miroshnichenko, M.A. Sheremet, I. Pop, A. Ishak, Convective heat transfer of micropolar fluid in a horizontal wavy channel under the local heating, *Int. J. Mech. Sci.* 128 (2017) 541–549.
- [11] A. Shenoy, M. Sheremet, I. Pop, Convective Flow and Heat Transfer from Wavy Surfaces: Viscous Fluids, Porous Media, and Nanofluids, CRC Press, 2016.
- [12] M. Bahiraei, N. Mazaheri, H. Moayedi, Employing v-shaped ribs and nanofluid as two passive methods to improve second law characteristics of flow within a square channel: a two-phase approach, *Int. J. Heat Mass Transf.* 151 (2020), 119419.
- [13] M. Parsaiehmehr, F. Pourfattah, O.A. Akbari, D. Toghraie, G. Sheikhzadeh, Turbulent flow and heat transfer of water/al₂O₃ nanofluid inside a rectangular ribbed channel, *Physica E* 96 (2018) 73–84.
- [14] S. Mosayebidorcheh, M. Hatami, Analytical investigation of peristaltic nanofluid flow and heat transfer in an asymmetric wavy wall channel (part I: straight channel), *Int. J. Heat Mass Transfer* 126 (2018) 790–799.
- [15] S. Mosayebidorcheh, M. Hatami, Analytical investigation of peristaltic nanofluid flow and heat transfer in an asymmetric wavy wall channel (part II: divergent channel), *Int. J. Heat Mass Transfer* 126 (2018) 800–808.
- [16] R. Dormohammadi, M. Farzaneh-Gord, A. Ebrahimi-Moghadam, M.H. Ahmadi, Heat transfer and entropy generation of the nanofluid flow inside sinusoidal wavy channels, *J. Mol. Liq.* 269 (2018) 229–240.
- [17] A.A.A.A. Alrashed, O.A. Akbari, A. Heydari, D. Toghraie, M. Zarringhalam, G.A. S. Shabani, et al., The numerical modeling of water/fmwcnt nanofluid flow and heat transfer in a backward-facing contracting channel, *Phys. B Condens. Matter* 537 (2018) 176–183.
- [18] D. Nouri, M. Pasandideh-Fard, M.J. Oboodi, O. Mahian, A.Z. Sahin, Entropy generation analysis of nanofluid flow over a spherical heat source inside a channel with sudden expansion and contraction, *Int. J. Heat Mass Transf.* 116 (2018) 1036–1043.
- [19] M.M. Ali, M.A. Alim, S.S. Ahmed, Oriented magnetic field effect on mixed convective flow of nanofluid in a grooved channel with internal rotating cylindrical heat source, *Int. J. Mech. Sci.* 151 (2019) 385–409.
- [20] V. Singh, D. Haridas, A. Srivastava, Experimental study of heat transfer performance of compact wavy channel with nanofluids as the coolant medium: real time non-intrusive measurements, *Int. J. Therm. Sci.* 145 (2019), 105993.
- [21] U. Akdag, S. Akcay, D. Demiral, Heat transfer enhancement with laminar pulsating nanofluid flow in a wavy channel, *Int. Communicat. Heat Mass Trans.* 59 (2014) 17–23.
- [22] M.A. Ahmed, M.Z. Yusoff, K.C. Ng, N.H. Shuaib, The effects of wavy-wall phase shift on thermal-hydraulic performance of al₂O₃-water nanofluid flow in sinusoidal-wavy channel, *Case Stud. Ther. Eng.* 4 (2014) 153–165.
- [23] Z. Alhajaj, A.M. Bayomy, M.Z. Saghir, M.M. Rahman, Flow of nanofluid and hybrid fluid in porous channels: Experimental and numerical approach, *Int. J. Thermo.* 100016 (2020).
- [24] H.R. Ashorynejad, A. Zarghami, Magneto hydrodynamics flow and heat transfer of cu-water nanofluid through a partially porous wavy channel, *Int. J. Heat Mass Transf.* 119 (2018) 247–258.
- [25] O. Manca, S. Nardini, D. Ricci, A numerical study of nanofluid forced convection in ribbed channels, *Appl. Therm. Eng.* 37 (2012) 280–292.
- [26] A. Andreozzi, O. Manca, S. Nardini, D. Ricci, Forced convection enhancement in channels with transversal ribs and nanofluids, *Appl. Therm. Eng.* 98 (2016) 1044–1053.
- [27] A.H. Rajabi, D. Toghraie, B. Mehandoust, Numerical simulation of turbulent nanofluid flow in the narrow channel with a heated wall and a spherical dimple placed on it by using of single-phase and mixture-phase models, *Int. Communicat. Heat Mass Trans.* 108 (2019), 104316.
- [28] A.S. Dalkç, O.A. Türk, H. Mercan, S. Nakkaew, S. Wongwises, An experimental investigation on heat transfer characteristics of graphite-sio₂/water hybrid nanofluid flow in horizontal tube with various quad-channel twisted tape inserts, *Int. Communicat. Heat Mass Trans.* 107 (2019) 1–13.
- [29] M. Khoshvaght-Aliabadi, M. Salami, Turbulent flow of al₂O₃-water nanofluid through plate-fin heat exchanger (PFHE) with offset-strip channels, *Thermal Sci Eng. Progress* 6 (2018) 164–176.
- [30] R.K. Ajeel, W.I. Salim, K. Hasnan, Thermal and hydraulic characteristics of turbulent nanofluids flow in trapezoidal-corrugated channel: symmetry and zigzag shaped, *Case Stud. Ther. Eng.* 12 (2018) 620–635.
- [31] R.K. Ajeel, W.I. Salim, K. Hasnan, Experimental and numerical investigations of convection heat transfer in corrugated channels using alumina nanofluid under a turbulent flow regime, *Chem. Eng. Res. Des.* 148 (2019) 202–217.
- [32] Z. Yin, F. Bao, C. Tu, Y. Hua, R. Tian, Numerical and experimental studies of heat and flow characteristics in a laminar pipe flow of nanofluid, *J. Exp. Nanosci.* 13 (1) (2018) 82–94.
- [33] M. Corcione, Empirical correlating equations for predicting the effective thermal conductivity and dynamic viscosity of nanofluids, *Energy Convers. Manag.* 52 (1) (2011) 789–793.
- [34] J.N. Reddy, *An Introduction to the Finite Element Method* vol. 2, McGraw-Hill, New York, 1993.
- [35] T.B. Gorji, A.A. Ranjbar, Geometry optimization of a nanofluid-based direct absorption solar collector using response surface methodology, *Sol. Energy* 122 (2015) 314–325.
- [36] M. Kalteh, A. Abbassi, M. Saffar-Avval, A. Frijns, A. Darhuber, J. Harting, Experimental and numerical investigation of nanofluid forced convection inside a wide microchannel heat sink, *Appl. Therm. Eng.* 36 (2012) 260–268.
- [37] E.M. Tokit, M.Z. Yusoff, H. Mohammed, Generality of brownian motion velocity of two phase approach in interrupted microchannel heat sink, *Int. Communicat Heat Mass Transfer* 49 (2013) 128–135.
- [38] T.L. Bergman, F.P. Incropera, *Introduction to Heat Transfer*, 6th edition, Wiley, New York, 2011.